

Measurement of Atmospheric Neutrino Oscillations at 6-56 GeV with IceCube DeepCore

M. G. Aartsen,² M. Ackermann,⁵² J. Adams,¹⁶ J. A. Aguilar,¹² M. Ahlers,²⁰ M. Ahrens,⁴⁴ I. Al Samarai,²⁵ D. Altmann,²⁴ K. Andeen,³³ T. Anderson,⁴⁹ I. Anseau,¹² G. Anton,²⁴ C. Argüelles,¹⁴ J. Auffenberg,¹ S. Axani,¹⁴ H. Bagherpour,¹⁶ X. Bai,⁴¹ J. P. Barron,²³ S. W. Barwick,²⁷ V. Baum,³² R. Bay,⁸ J. J. Beatty,^{18, 19} J. Becker Tjus,¹¹ K.-H. Becker,⁵¹ S. BenZvi,⁴³ D. Berley,¹⁷ E. Bernardini,⁵² D. Z. Besson,²⁸ G. Binder,^{9, 8} D. Bindig,⁵¹ E. Blaufuss,¹⁷ S. Blot,⁵² C. Boehm,⁴⁴ M. Börner,²¹ F. Bos,¹¹ D. Bose,⁴⁶ S. Böser,³² O. Botner,⁵⁰ J. Bourbeau,³¹ F. Bradascio,⁵² J. Braun,³¹ L. Brayer,¹³ M. Brenzke,¹ H.-P. Bretz,⁵² S. Bron,²⁵ J. Brostean-Kaiser,⁵² A. Burgman,⁵⁰ T. Carver,²⁵ J. Casey,³¹ M. Casier,¹³ E. Cheung,¹⁷ D. Chirkin,³¹ A. Christov,²⁵ K. Clark,²⁹ L. Classen,³⁶ S. Coenders,³⁵ G. H. Collin,¹⁴ J. M. Conrad,¹⁴ D. F. Cowen,^{49, 48} R. Cross,⁴³ M. Day,³¹ J. P. A. M. de André,²² C. De Clercq,¹³ J. J. DeLaunay,⁴⁹ H. Dembinski,³⁷ S. De Ridder,²⁶ P. Desiati,³¹ K. D. de Vries,¹³ G. de Wasseige,¹³ M. de With,¹⁰ T. DeYoung,²² J. C. Díaz-Vélez,³¹ V. di Lorenzo,³² H. Dujmovic,⁴⁶ J. P. Dumm,⁴⁴ M. Dunkman,⁴⁹ B. Eberhardt,³² T. Ehrhardt,³² B. Eichmann,¹¹ P. Eller,⁴⁹ P. A. Evenson,³⁷ S. Fahey,³¹ A. R. Fazely,⁷ J. Felde,¹⁷ K. Filimonov,⁸ C. Finley,⁴⁴ S. Flis,⁴⁴ A. Franckowiak,⁵² E. Friedman,¹⁷ T. Fuchs,²¹ T. K. Gaisser,³⁷ J. Gallagher,³⁰ L. Gerhardt,⁹ K. Ghorbani,³¹ W. Giang,²³ T. Glauch,¹ T. Glüsenkamp,²⁴ A. Goldschmidt,⁹ J. G. Gonzalez,³⁷ D. Grant,²³ Z. Griffith,³¹ C. Haack,¹ A. Hallgren,⁵⁰ F. Halzen,³¹ K. Hanson,³¹ D. Hebecker,¹⁰ D. Heereman,¹² K. Helbing,⁵¹ R. Hellauer,¹⁷ S. Hickford,⁵¹ J. Hignight,²² G. C. Hill,² K. D. Hoffman,¹⁷ R. Hoffmann,⁵¹ B. Hokanson-Fasig,³¹ K. Hoshina,^{31, *} F. Huang,⁴⁹ M. Huber,³⁵ K. Hultqvist,⁴⁴ M. Hünnefeld,²¹ S. In,⁴⁶ A. Ishihara,¹⁵ E. Jacobi,⁵² G. S. Japaridze,⁵ M. Jeong,⁴⁶ K. Jero,³¹ B. J. P. Jones,⁴ P. Kalaczynski,¹ W. Kang,⁴⁶ A. Kappes,³⁶ T. Karg,⁵² A. Karle,³¹ U. Katz,²⁴ M. Kauer,³¹ A. Keivani,⁴⁹ J. L. Kelley,³¹ A. Kheirandish,³¹ J. Kim,⁴⁶ M. Kim,¹⁵ T. Kintscher,⁵² J. Kiryluk,⁴⁵ T. Kittler,²⁴ S. R. Klein,^{9, 8} G. Kohlen,³⁴ R. Koirala,³⁷ H. Kolanoski,¹⁰ L. Köpke,³² C. Kopper,²³ S. Kopper,⁴⁷ J. P. Koschinsky,¹ D. J. Koskinen,²⁰ M. Kowalski,^{10, 52} K. Krings,³⁵ M. Kroll,¹¹ G. Krückl,³² J. Kunnen,¹³ S. Kunwar,⁵² N. Kurahashi,⁴⁰ T. Kuwabara,¹⁵ A. Kyriacou,² M. Labare,²⁶ J. L. Lanfranchi,⁴⁹ M. J. Larson,²⁰ F. Lauber,⁵¹ D. Lennarz,²² M. Lesiak-Bzdak,⁴⁵ M. Leuermann,¹ Q. R. Liu,³¹ L. Lu,¹⁵ J. Lünemann,¹³ W. Luszczak,³¹ J. Madsen,⁴² G. Maggi,¹³ K. B. M. Mahn,²² S. Mancina,³¹ R. Maruyama,³⁸ K. Mase,¹⁵ R. Maunu,¹⁷ F. McNally,³¹ K. Meagher,¹² M. Medici,²⁰ M. Meier,²¹ T. Menne,²¹ G. Merino,³¹ T. Meures,¹² S. Miarecki,^{9, 8} J. Micallef,²² G. Momenté,³² T. Montaruli,²⁵ R. W. Moore,²³ M. Moulai,¹⁴ R. Nahnauer,⁵² P. Nakarmi,⁴⁷ U. Naumann,⁵¹ G. Neer,²² H. Niederhausen,⁴⁵ S. C. Nowicki,²³ D. R. Nygren,⁹ A. Obertacke Pollmann,⁵¹ A. Olivas,¹⁷ A. O'Murchadha,¹² T. Palczewski,^{9, 8} H. Pandya,³⁷ D. V. Pankova,⁴⁹ P. Peiffer,³² J. A. Pepper,⁴⁷ C. Pérez de los Heros,⁵⁰ D. Pieloth,²¹ E. Pinat,¹² M. Plum,³³ P. B. Price,⁸ G. T. Przybylski,⁹ C. Raab,¹² L. Rädcl,¹ M. Rameez,²⁰ K. Rawlins,³ I. C. Rea,³⁵ R. Reimann,¹ B. Relethford,⁴⁰ M. Relich,¹⁵ E. Resconi,³⁵ W. Rhode,²¹ M. Richman,⁴⁰ S. Robertson,² M. Rongen,¹ C. Rott,⁴⁶ T. Ruhe,²¹ D. Ryckbosch,²⁶ D. Rysewyk,²² T. Sälzer,¹ S. E. Sanchez Herrera,²³ A. Sandrock,²¹ J. Sandroos,³² S. Sarkar,^{20, 39} S. Sarkar,²³ K. Satalecka,⁵² P. Schlunder,²¹ T. Schmidt,¹⁷ A. Schneider,³¹ S. Schoenen,¹ S. Schöneberg,¹¹ L. Schumacher,¹ D. Seckel,³⁷ S. Seunarine,⁴² J. Soedingrekso,²¹ D. Soldin,⁵¹ M. Song,¹⁷ G. M. Spiczak,⁴² C. Spiering,⁵² J. Stachurska,⁵² M. Stamatikos,¹⁸ T. Stanev,³⁷ A. Stasik,⁵² J. Stettner,¹ A. Steuer,³² T. Stezelberger,⁹ R. G. Stokstad,⁹ A. Stöbl,¹⁵ N. L. Strotjohann,⁵² G. W. Sullivan,¹⁷ M. Sutherland,¹⁸ I. Taboada,⁶ J. Tatar,^{9, 8} F. Tenholt,¹¹ S. Ter-Antonyan,⁷ A. Terliuk,⁵² G. Tešić,⁴⁹ S. Tilav,³⁷ P. A. Toale,⁴⁷ M. N. Tobin,³¹ S. Toscano,¹³ D. Tosi,³¹ M. Tselengidou,²⁴ C. F. Tung,⁶ A. Turcati,³⁵ C. F. Turley,⁴⁹ B. Ty,³¹ E. Unger,⁵⁰ M. Usner,⁵² J. Vandenbroucke,³¹ W. Van Driessche,²⁶ N. van Eijndhoven,¹³ S. Vanheule,²⁶ J. van Santen,⁵² M. Vehring,¹ E. Vogel,¹ M. Vraeghe,²⁶ C. Walck,⁴⁴ A. Wallace,² M. Wallraff,¹ F. D. Wandler,²³ N. Wandkowsky,³¹ A. Waza,¹ C. Weaver,²³ M. J. Weiss,⁴⁹ C. Wendt,³¹ J. Werthebach,²¹ S. Westerhoff,³¹ B. J. Whelan,² K. Wiebe,³² C. H. Wiebusch,¹ L. Wille,³¹ D. R. Williams,⁴⁷ L. Wills,⁴⁰ M. Wolf,³¹ J. Wood,³¹ T. R. Wood,²³ E. Woolsey,²³ K. Woschnagg,⁸ D. L. Xu,³¹ X. W. Xu,⁷ Y. Xu,⁴⁵ J. P. Yanez,²³ G. Yodh,²⁷ S. Yoshida,¹⁵ T. Yuan,³¹ and M. Zoll⁴⁴

(IceCube Collaboration)

¹*III. Physikalisches Institut, RWTH Aachen University, D-52056 Aachen, Germany*

²*Department of Physics, University of Adelaide, Adelaide, 5005, Australia*

³*Dept. of Physics and Astronomy, University of Alaska Anchorage, 3211 Providence Dr., Anchorage, AK 99508, USA*

⁴*Dept. of Physics, University of Texas at Arlington, 502 Yates St., Science Hall Rm 108, Box 19059, Arlington, TX 76019, USA*

- ⁵CTSPS, Clark-Atlanta University, Atlanta, GA 30314, USA
⁶School of Physics and Center for Relativistic Astrophysics,
Georgia Institute of Technology, Atlanta, GA 30332, USA
⁷Dept. of Physics, Southern University, Baton Rouge, LA 70813, USA
⁸Dept. of Physics, University of California, Berkeley, CA 94720, USA
⁹Lawrence Berkeley National Laboratory, Berkeley, CA 94720, USA
¹⁰Institut für Physik, Humboldt-Universität zu Berlin, D-12489 Berlin, Germany
¹¹Fakultät für Physik & Astronomie, Ruhr-Universität Bochum, D-44780 Bochum, Germany
¹²Université Libre de Bruxelles, Science Faculty CP230, B-1050 Brussels, Belgium
¹³Vrije Universiteit Brussel (VUB), Dienst ELEM, B-1050 Brussels, Belgium
¹⁴Dept. of Physics, Massachusetts Institute of Technology, Cambridge, MA 02139, USA
¹⁵Dept. of Physics and Institute for Global Prominent Research, Chiba University, Chiba 263-8522, Japan
¹⁶Dept. of Physics and Astronomy, University of Canterbury, Private Bag 4800, Christchurch, New Zealand
¹⁷Dept. of Physics, University of Maryland, College Park, MD 20742, USA
¹⁸Dept. of Physics and Center for Cosmology and Astro-Particle Physics,
Ohio State University, Columbus, OH 43210, USA
¹⁹Dept. of Astronomy, Ohio State University, Columbus, OH 43210, USA
²⁰Niels Bohr Institute, University of Copenhagen, DK-2100 Copenhagen, Denmark
²¹Dept. of Physics, TU Dortmund University, D-44221 Dortmund, Germany
²²Dept. of Physics and Astronomy, Michigan State University, East Lansing, MI 48824, USA
²³Dept. of Physics, University of Alberta, Edmonton, Alberta, Canada T6G 2E1
²⁴Erlangen Centre for Astroparticle Physics, Friedrich-Alexander-Universität Erlangen-Nürnberg, D-91058 Erlangen, Germany
²⁵Département de physique nucléaire et corpusculaire,
Université de Genève, CH-1211 Genève, Switzerland
²⁶Dept. of Physics and Astronomy, University of Gent, B-9000 Gent, Belgium
²⁷Dept. of Physics and Astronomy, University of California, Irvine, CA 92697, USA
²⁸Dept. of Physics and Astronomy, University of Kansas, Lawrence, KS 66045, USA
²⁹SNOLAB, 1039 Regional Road 24, Creighton Mine 9, Lively, ON, Canada P3Y 1N2
³⁰Dept. of Astronomy, University of Wisconsin, Madison, WI 53706, USA
³¹Dept. of Physics and Wisconsin IceCube Particle Astrophysics Center,
University of Wisconsin, Madison, WI 53706, USA
³²Institute of Physics, University of Mainz, Staudinger Weg 7, D-55099 Mainz, Germany
³³Department of Physics, Marquette University, Milwaukee, WI, 53201, USA
³⁴Université de Mons, 7000 Mons, Belgium
³⁵Physik-department, Technische Universität München, D-85748 Garching, Germany
³⁶Institut für Kernphysik, Westfälische Wilhelms-Universität Münster, D-48149 Münster, Germany
³⁷Bartol Research Institute and Dept. of Physics and Astronomy,
University of Delaware, Newark, DE 19716, USA
³⁸Dept. of Physics, Yale University, New Haven, CT 06520, USA
³⁹Dept. of Physics, University of Oxford, 1 Keble Road, Oxford OX1 3NP, UK
⁴⁰Dept. of Physics, Drexel University, 3141 Chestnut Street, Philadelphia, PA 19104, USA
⁴¹Physics Department, South Dakota School of Mines and Technology, Rapid City, SD 57701, USA
⁴²Dept. of Physics, University of Wisconsin, River Falls, WI 54022, USA
⁴³Dept. of Physics and Astronomy, University of Rochester, Rochester, NY 14627, USA
⁴⁴Oskar Klein Centre and Dept. of Physics, Stockholm University, SE-10691 Stockholm, Sweden
⁴⁵Dept. of Physics and Astronomy, Stony Brook University, Stony Brook, NY 11794-3800, USA
⁴⁶Dept. of Physics, Sungkyunkwan University, Suwon 440-746, Korea
⁴⁷Dept. of Physics and Astronomy, University of Alabama, Tuscaloosa, AL 35487, USA
⁴⁸Dept. of Astronomy and Astrophysics, Pennsylvania State University, University Park, PA 16802, USA
⁴⁹Dept. of Physics, Pennsylvania State University, University Park, PA 16802, USA
⁵⁰Dept. of Physics and Astronomy, Uppsala University, Box 516, S-75120 Uppsala, Sweden
⁵¹Dept. of Physics, University of Wuppertal, D-42119 Wuppertal, Germany
⁵²DESY, D-15738 Zeuthen, Germany

(Dated: July 25, 2017)

We present a measurement of the atmospheric neutrino oscillation parameters using three years of data from the IceCube Neutrino Observatory. The DeepCore infill array in the center of IceCube enables detection and reconstruction of neutrinos produced by the interaction of cosmic rays in the Earth's atmosphere at energies as low as ~ 5 GeV. That energy threshold permits measurements of muon neutrino disappearance, over a range of baselines up to the diameter of the Earth, probing the same range of L/E_ν as long-baseline experiments but with substantially higher energy neutrinos. This analysis uses neutrinos from the full sky with reconstructed energies from 5.6 – 56 GeV. We measure $\Delta m_{32}^2 = 2.31_{-0.13}^{+0.11} \times 10^{-3} \text{ eV}^2$ and $\sin^2 \theta_{23} = 0.51_{-0.09}^{+0.07}$, assuming normal neutrino mass

ordering. These results are consistent with, and of similar precision to, those from accelerator and reactor-based experiments.

INTRODUCTION

It has been well established that the neutrino mass eigenstates do not correspond to the neutrino flavor eigenstates, leading to flavor oscillations as neutrinos propagate through space [1, 2]. After traveling a distance L a neutrino of energy E may be detected with a different flavor than it was produced with. In particular, the muon neutrino survival probability is described approximately by

$$P(\nu_\mu \rightarrow \nu_\mu) \approx 1 - 4|U_{\mu 3}|^2 (1 - |U_{\mu 3}|^2) \sin^2 \left(\frac{\Delta m_{32}^2 L}{4E} \right), \quad (1)$$

where $U_{\mu 3} = \sin \theta_{23} \cos \theta_{13}$ is one element of the PMNS [3, 4] matrix U expressed in terms of the mixing angles θ_{23} and θ_{13} , $\Delta m_{32}^2 = m_3^2 - m_2^2$ is the splitting of the second and third neutrino mass states that drives oscillation on the length and energy scales relevant to this analysis. In addition to the parameters shown in Eq. (1), neutrino oscillations also depend on the parameters θ_{12} , Δm_{21}^2 and δ_{CP} , but these have a negligible effect on the data presented in this paper.

Atmospheric neutrinos produced by the interaction of cosmic rays in the atmosphere [5–7] provide a large flux of neutrinos traveling distances ranging from $L \sim 20$ km (vertically down-going) to $L \sim 1.3 \times 10^4$ km (vertically up-going) to a detector near the Earth’s surface. For these up-going neutrinos, there is a maximum muon neutrino disappearance at energies as high as ~ 25 GeV. Given the density of material traversed by these neutrinos, matter effects alter Eq. (1) slightly and must be taken into account [8–11].

In this letter, we report our measurement of θ_{23} and Δm_{32}^2 using the IceCube Observatory. This measurement was obtained by observing the oscillation-induced patterns in the atmospheric neutrino flux coming from all directions between 5.6 GeV and 56 GeV. The results presented here complement other leading experiments [12–16] in two ways. Long-baseline experiments with baselines of a few hundred kilometers and Super-Kamiokande observe much lower energy events (primarily charged-current quasi-elastic and resonant scattering), while our data consist almost entirely of higher energy deep inelastic scattering events and are thus subject to different sources of systematic uncertainty [17]. In addition, the higher energy range of IceCube neutrinos can provide complementary constraints on potential new physics in the neutrino sector [18–27].

The IceCube detector was fully commissioned in 2011 and IceCube previously reported results [28] that used data from May 2011 through April 2014. The previous results were obtained using reconstruction tools that relied

on detecting unscattered Cherenkov photons and therefore are less susceptible to detector noise. The results presented here were obtained with a new reconstruction that includes scattered photons and retains an order of magnitude more events per year. Because the detector’s noise rates were still stabilizing during the first year of operation, and the new reconstruction is more susceptible to noise, this result is based on data from April 2012 through May 2015.

THE ICECUBE DEEPCORE DETECTOR

The IceCube In-Ice Array [29] is composed of 5160 downward-looking 10” photomultiplier tubes (PMTs) buried in the South Pole glacial ice at depths between 1.45 and 2.45 km, instrumenting a volume of 1 km³. These PMTs and their associated electronics are enclosed in glass pressure spheres to form digital optical modules (DOMs) [30, 31]. The DOMs are deployed on 86 vertical strings with 60 modules per string. Of those strings, 78 are deployed in a triangular grid, with a distance of about 125 m between neighboring strings. In this analysis, these DOMs are used primarily as an active veto to reject atmospheric muon contaminations in the sample. The remaining 8 strings fill $\sim 10^7$ m³ of ice in the bottom center of the detector with denser instrumentation. Data from this region, called DeepCore, are used in this analysis as the denser instrumentation enables detection of neutrinos with energies down to ~ 5 GeV [32].

Neutrino interactions in DeepCore are simulated with GENIE [33]. Hadrons produced in these interactions are simulated using GEANT4 [34], as are electromagnetic showers below 100 MeV. At higher energies, shower-to-shower variation is small enough to permit the use of standardized light emission templates [35] based on GEANT4 simulations to reduce computation time. Muons energy losses in the ice are simulated using the PROPOSAL package [36]. Cherenkov photons produced by showers and muons are tracked individually using GPU-based software to simulate scattering and absorption [37].

RECONSTRUCTION AND EVENT SELECTION

The event reconstruction used in this analysis models the scattering of Cherenkov photons in the ice surrounding our DOMs [38] to calculate the likelihood of the observed photoelectrons as a function of the neutrino interaction position, direction, and energy. Given the complexity of this likelihood space, the MultiNest algorithm [39] is used to find the global maximum. This

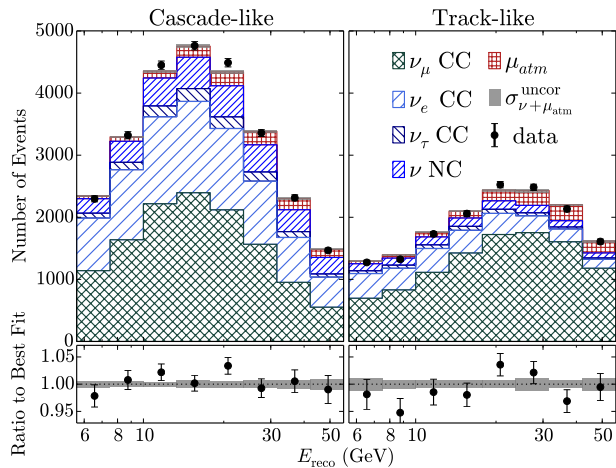


FIG. 1. Reconstructed energy distributions observed in data (points) and predicted by interaction type at our best fit point for oscillations (stacked). In addition to each separate component, the uncorrelated statistical uncertainty associated to the expectation ($\sigma_{\nu+\mu_{\text{atm}}}^{\text{uncor}}$) is shown in a shaded band. The track-like sample is peaked at higher energy due to the rising probability of tagging ν_{μ} CC events. The bottom plots show the ratio of the data to the fitted prediction.

reconstruction is run using two different event hypotheses: once assuming a ν_{μ} charged-current (CC) interaction comprising a hadronic shower and a collinear muon track emerging from the interaction vertex, and once with only a shower at the vertex, which is a nested hypothesis of the first reconstruction if the muon track length was zero. The latter model incorporates ν_e and most ν_{τ} CC interactions as well as neutral current interactions, as we do not attempt to separate the electromagnetic shower produced by the leading lepton from the hadronic shower produced by the disrupted nucleus.

The ν_{μ} CC reconstruction is used to estimate the direction and energy of the neutrinos. The difference in best-fit likelihoods between the two hypotheses is used to classify our events as “track-like,” if inclusion of a muon improves the fitting result substantially, or “cascade-like,” if the event is equally well described without a muon. The distributions of events in each of these categories after final selection are shown in Fig. 1 as a function of reconstructed neutrino energy (E_{reco}), with the corresponding predicted distributions broken down by event interaction type. The track-like sample is enriched in ν_{μ} CC events (68% of sample), especially at higher energies where muons are more likely detected, while the cascade-like sample is evenly divided between ν_{μ} CC and interactions without a muon in the final state. The angular and energy resolutions provided by the reconstruction are energy-dependent, with median resolutions of 10° (16°) in zenith angle and 24% (29%) in neutrino energy for track-like (cascade-like) events at $E_{\nu} = 20$ GeV.

The event selection used in this analysis uses the IceCube DOMs surrounding the DeepCore region as an active veto against atmospheric muons. The first selection criteria remove accidental triggers caused by dark noise by demanding a minimum amount of light detected in the DeepCore volume, with timing and spatial scale consistent with a particle emitting Cherenkov radiation. Events in which photons are observed outside the DeepCore volume, in a time window consistent with atmospheric muons penetrating to the fiducial volume, are also rejected. These are followed by a boosted decision tree (BDT) [40] which further reduces the background of atmospheric muons. The BDT uses the timing and spatial scale of the detected photoelectrons to select events with substantial charge deposition at the beginning of the event, indicative of a neutrino interaction vertex. It also considers how close the event is to the border of the DeepCore volume and the results of several fast directional reconstructions [41] in determining whether the event may be an atmospheric muon. Finally, we demand the interaction vertex reconstructed by the likelihood algorithm described above be contained within DeepCore and the end of the reconstructed muon is within the first row of DOMs outside DeepCore, to further reduce atmospheric muon contamination and to improve the accuracy of the reconstruction.

As these selection criteria reduce the atmospheric muon rate by a factor of approximately 10^8 , it is challenging to simulate enough atmospheric muons to obtain a reliable prediction for the distribution of the remaining muons, especially in the presence of systematic uncertainties. We instead use a data-driven estimate of the shape of the muon background distributions, with the normalization free to float. This approach is based on tagging events that would have been accepted except for a small number of photons detected in the veto region, similar to the procedure in Ref. [28]. The uncertainty in the background shape is estimated using two different criteria for tagging these events and was compared to the currently available muon Monte Carlo. This uncertainty is added in quadrature to the statistical uncertainties in the tagged background event sample and the neutrino Monte Carlo, to provide the total uncorrelated statistical uncertainty ($\sigma_{\nu+\mu_{\text{atm}}}^{\text{uncor}}$) in the expected event distribution shown in Fig. 1.

ANALYSIS

The final fit of the data is done using an $8 \times 8 \times 2$ binned histogram, with 8 bins in $\log_{10} E_{\text{reco}}$, 8 bins in the cosine of the reconstructed neutrino zenith direction ($\cos \theta_{z,\text{reco}}$), one track-like bin and one cascade-like. The bins are equally spaced with $\cos \theta_{z,\text{reco}} \in [-1, 1]$ and $\log_{10} E_{\text{reco}} \in [0.75, 1.75]$. The fit assumes three-flavor os-

cillations with $\Delta m_{21}^2 = 7.53 \times 10^{-5} \text{ eV}^2$, $\sin^2 \theta_{12} = 0.304$, $\sin^2 \theta_{13} = 2.17 \times 10^{-2}$, and $\delta_{CP} = 0^\circ$.

We use MINUIT2 [42] to minimize a χ^2 function defined as

$$\chi^2 = \sum_{i \in \{\text{bins}\}} \frac{(n_i^{\nu+\mu_{\text{atm}}} - n_i^{\text{data}})^2}{(\sigma_i^{\text{data}})^2 + (\sigma_{\nu+\mu_{\text{atm}},i}^{\text{uncor}})^2} + \sum_{j \in \{\text{syst}\}} \frac{(s_j - \hat{s}_j)^2}{\hat{\sigma}_{s_j}^2}, \quad (2)$$

where $n_i^{\nu+\mu_{\text{atm}}}$ is the number of events expected in the i^{th} bin, which is the sum of neutrino events weighted to the desired oscillation parameters using Prob3++ [43] and the atmospheric muon background. The number of events observed in the i^{th} bin is n_i^{data} , with Poisson uncertainty $\sigma_i^{\text{data}} = \sqrt{n_i^{\text{data}}}$, and $\sigma_{\nu+\mu_{\text{atm}},i}^{\text{uncor}}$ is the uncertainty in the prediction of the number of events of the i^{th} bin. $\sigma_{\nu+\mu_{\text{atm}}}^{\text{uncor}}$ includes both uncertainty due to finite MC statistics and the uncertainties in our data-driven muon background estimate described above. The second term of Eq. (2) is the penalty term for our nuisance parameters, where s_j is the value of j^{th} systematic, \hat{s}_j is the central value and $\hat{\sigma}_{s_j}^2$ is the Gaussian standard deviation of the j^{th} systematic prior.

The analysis includes eleven nuisance parameters describing our systematic uncertainties, summarized in Table I. Seven parameters are related to systematic uncertainties in the atmospheric neutrino flux and interaction cross sections. Since only the event rate is observed directly, some uncertainties in flux and cross section have similar effects on the data. In these cases, the degenerate effects are combined into a single parameter. Because analytical models of these effects are available, these parameters can be varied continuously by weighting simulated events.

The first nuisance parameter is the overall normalization of the event rate. It is affected by uncertainties in the atmospheric neutrino flux, in the neutrino interaction cross section, and by the possibility of accidentally vetoing neutrino events due to unrelated atmospheric muons detected in the veto volume. This last effect is expected to reduce the neutrino rate by several percent, but is not included in the present simulations. A second parameter allows an energy-dependent shift in the event rate. This can arise from uncertainty on the spectral index of the atmospheric flux (nominally $\gamma = -2.66$ at the relevant energies in our neutrino flux model [7]), or from uncertainties in the deep inelastic scattering (DIS) cross section.

Detailed studies of DIS uncertainties found them to be either highly degenerate with changes in the normalization and spectral index of the atmospheric neutrino flux over the energy range of this analysis, or to be negligible. The studies included variation of parameters of the Bodek-Yang model [44] used in GENIE, uncertainties in the differential cross-section of DIS neutrino scattering, and studies of hadronization uncertainties for high- W DIS events [45]. As these effects are well described by

TABLE I. Table of nuisance parameters along with their associated priors, if applicable. The right two columns show the results from our best fit for normal mass ordering and inverted mass ordering, respectively.

Parameters	Priors	Best Fit	
		NO	IO
Flux and cross section parameters			
Neutrino event rate [% of nominal]	no prior	85	85
$\Delta\gamma$ (spectral index)	0.00 ± 0.10	-0.02	-0.02
M_A (resonance) [GeV]	1.12 ± 0.22	0.92	0.93
$\nu_e + \bar{\nu}_e$ relative normalization [%]	100 ± 20	125	125
NC relative normalization [%]	100 ± 20	106	106
$\Delta(\nu/\bar{\nu})$ [σ], energy dependent [46]	0.00 ± 1.00	-0.56	-0.59
$\Delta(\nu/\bar{\nu})$ [σ], zenith dependent [46]	0.00 ± 1.00	-0.55	-0.57
Detector parameters			
overall optical eff. [%]	100 ± 10	102	102
relative optical eff., lateral [σ]	0.0 ± 1.0	0.2	0.2
relative optical eff., head-on [a.u.]	no prior	-0.72	-0.66
Background			
Atm. μ contamination [% of sample]	no prior	5.5	5.6

the first two nuisance parameters, additional nuisance parameters were unnecessary. A prior of $\hat{\sigma}_s = 0.10$ is placed on the spectral index to describe the range of these uncertainties; no prior was imposed on the rate normalization.

One neutrino cross-section uncertainty was not well described by these parameters: the uncertainty of the axial mass form factor for resonant events. The default value of 1.12 GeV and prior of 0.22 GeV were taken from GENIE [33]. Uncertainties in CCQE interactions were also investigated but had no impact on the analysis due to the relatively small percentage of CCQE events at these energies.

The normalizations of $\nu_e + \bar{\nu}_e$ events and of NC events, defined relative to $\nu_\mu + \bar{\nu}_\mu$ CC events, are both assigned an uncertainty of 20%. Uncertainties in the relative contributions of neutrino and anti-neutrino events are split into two parameters, one dependent on energy and the other on the zenith angle. These last two uncertainties are parameterized from Ref. [46].

Systematics related to the response of the detector itself have the largest impact on this analysis. Their effects are estimated by Monte Carlo simulation at discrete values, with the contents of each bin in the (energy, direction, track/cascade) analysis histogram determined by linear interpolation between the discrete simulated values, following the approach of Ref. [27, 28].

Uncertainties in the efficiency of photon detection are driven by the formation of bubbles in the refrozen ice columns in the holes where the IceCube strings were deployed. A prior with a width of 10% was applied to the overall photon collection efficiency [29], parameterized using seven MC data sets ranging from 88% to 112% of the nominal optical efficiency. In addition to modifying the absolute efficiency, these bubbles can scatter Cherenkov photons near the DOMs, modulating the relative opti-

cal efficiency as function of the incident photon angle. The effect of the refrozen ice column is modeled by two effective parameters controlling the shape of the DOM angular acceptance curve.

The first parameter controls the lateral angular acceptance (i.e., relative sensitivity to photons traveling roughly 20° above versus below the horizontal) and is relatively well constrained by LED calibration data. Five MC data sets were generated covering the -1σ to $+1\sigma$ uncertainty from the LED calibration, and parametrized in the same way as the overall optical efficiency described above. A Gaussian prior based on the calibration data is applied.

The second parameter controls sensitivity to photons traveling vertically upward and striking the DOMs head-on, and is not well constrained by string-to-string LED calibration. That effect is modeled using a dimensionless parameter ranging from -5 (corresponding to a bubble column completely obscuring the DOM face for vertically incident photons) to 2.5 (no obscuration). A value of zero corresponds to constant sensitivity for angles of incidence from 0° to 30° from vertical. Six MC sets covering the range from -5 to 2 were used to parametrize this effect. No prior is used for this parameter due to lack of information from calibration data.

The last nuisance parameter controls the amount of atmospheric muon contamination in the final data sample. As described above, a data-driven method is used to estimate the shape of this background in the analysis histogram, including binwise uncertainties. Since the absolute efficiency for tagging background events with this method is unknown, the normalization of the muon contribution is left free in the fit.

In addition to the systematic uncertainties discussed above, we have considered the impact of seed dependence in our event reconstruction, different optical models for both the undisturbed ice and the refrozen ice columns, and an improved detector calibration currently being prepared. In all these cases the impact on the final result was found to be minor, and they were thus omitted from the fit and the error calculation.

RESULTS AND CONCLUSION

The analysis procedure described above gives a best fit of $\Delta m_{32}^2 = 2.31_{-0.13}^{+0.11} \times 10^{-3} \text{ eV}^2$ and $\sin^2 \theta_{23} = 0.51_{-0.09}^{+0.07}$, assuming normal neutrino mass ordering. For the inverted mass ordering, the best fit shifts to $\Delta m_{32}^2 = -2.32 \times 10^{-3} \text{ eV}^2$ and $\sin^2 \theta_{23} = 0.51$. The pulls on the nuisance parameters can be found in Table I. Our results are still statistics limited.

The data agree well with the best-fit MC data set, with a χ^2 of 117.4 for both neutrino mass orderings. This corresponds to a p-value of 0.52 given the 119 effective degrees of freedom estimated via toy MCs, following the

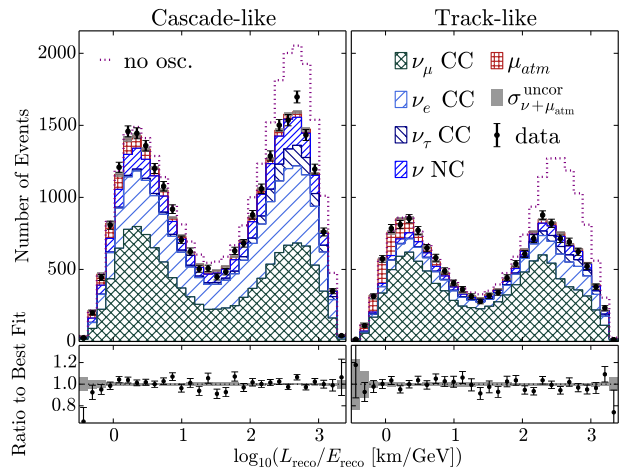


FIG. 2. Data projected onto L/E for illustration. The black dots indicate the data along with their corresponding statistical errors. The dotted line shows the expectation in the absence of neutrino oscillations. The stacked hatched histograms are the predicted counts given the best-fit values of all parameters in the fit for each component. The $\sigma_{\nu+\mu_{atm}}^{\text{uncor}}$ uncertainty as defined in Eq. (2) is also shown. The bottom plots show the ratio of the data to the fitted prediction.

procedure described in Ref. [27].

To better visualize the fit, Fig. 2 shows the results of the fit projected onto a single L/E axis, for both the track-like and cascade-like events. The two peaks in each distribution correspond to down-going and up-going neutrino trajectories. Up-going $\nu_\mu + \bar{\nu}_\mu$ are strongly suppressed in the track-like channel due to oscillations. Some suppression of up-going cascade-like data is also visible, due to disappearance of lower-energy ν_μ which are not tagged as track-like events by our reconstruction.

Figure 3 shows the region of $\sin^2 \theta_{23}$ and Δm_{32}^2 allowed by our analysis at 90% C.L., along with our best-fit point and several other leading measurements of these parameters [12–14, 16]. The contours are calculated using the approach of Feldman and Cousins [47] to ensure proper coverage.

Our results are consistent with those from other experiments [12–16], albeit with significantly higher energy neutrinos and are subject to a different set of systematic uncertainties. Our data prefer maximal mixing, similar to the result from T2K [13]. The best-fit values from the NO ν A experiment [14] are disfavored by $\Delta\chi^2 = 8.9$ (first octant) or $\Delta\chi^2 = 8.8$ (second octant), corresponding to a significance of 2.6σ using the method of Feldman and Cousins, although there is considerable overlap in the 90% confidence regions of the two measurements. Further improvements to our analysis are underway, including the incorporation of additional years of data, ongoing extensions of our event selections, and improved calibration of the detector response.

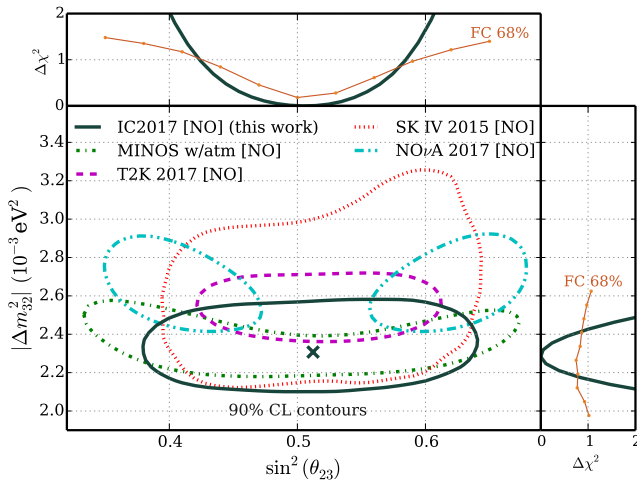


FIG. 3. The 90% allowed region from this work (solid line) compared to other experiments [12–14, 16] (dashed lines). The cross marks our best-fit point. The outer plots show the results of the 1-D projections after profiling over the other variables along with the 68% CL $\Delta\chi^2_c$ threshold estimated using the Feldman-Cousins method [47].

ACKNOWLEDGEMENTS

We acknowledge the support from the following agencies: U.S. National Science Foundation-Office of Polar Programs, U.S. National Science Foundation-Physics Division, University of Wisconsin Alumni Research Foundation, Michigan State University, the Grid Laboratory Of Wisconsin (GLOW) grid infrastructure at the University of Wisconsin - Madison, the Open Science Grid (OSG) grid infrastructure; U.S. Department of Energy, and National Energy Research Scientific Computing Center, the Louisiana Optical Network Initiative (LONI) grid computing resources; Natural Sciences and Engineering Research Council of Canada, WestGrid and Compute/Calcul Canada; Swedish Research Council, Swedish Polar Research Secretariat, Swedish National Infrastructure for Computing (SNIC), and Knut and Alice Wallenberg Foundation, Sweden; German Ministry for Education and Research (BMBF), Deutsche Forschungsgemeinschaft (DFG), Helmholtz Alliance for Astroparticle Physics (HAP), Initiative and Networking Fund of the Helmholtz Association, Germany; Fund for Scientific Research (FNRS-FWO), FWO Odysseus programme, Flanders Institute to encourage scientific and technological research in industry (IWT), Belgian Federal Science Policy Office (Belspo); Marsden Fund, New Zealand; Australian Research Council; Japan Society for Promotion of Science (JSPS); the Swiss National Science Foundation (SNSF), Switzerland; National Research Foundation of Korea (NRF); Villum Fonden, Danish National Research Foundation (DNRF), Denmark

- * Earthquake Research Institute, University of Tokyo, Bunkyo, Tokyo 113-0032, Japan
- [1] Y. Fukuda et al. (Super-Kamiokande), *Phys. Rev. Lett.* **81**, 1562 (1998), hep-ex/9807003.
 - [2] Q. R. Ahmad et al. (SNO), *Phys. Rev. Lett.* **87**, 071301 (2001), nucl-ex/0106015.
 - [3] B. Pontecorvo, *Sov. Phys. JETP* **6**, 429 (1957), [*Zh. Eksp. Teor. Fiz.* 33,549(1957)].
 - [4] Z. Maki, M. Nakagawa, and S. Sakata, *Prog. Theor. Phys.* **28**, 870 (1962).
 - [5] L. V. Volkova, *Sov. J. Nucl. Phys.* **31**, 784 (1980), [*Yad. Fiz.* 31,1510(1980)].
 - [6] G. D. Barr, T. K. Gaisser, P. Lipari, S. Robbins, and T. Stanev, *Phys. Rev.* **D70**, 023006 (2004), astro-ph/0403630.
 - [7] M. Honda, M. Sajjad Athar, T. Kajita, K. Kasahara, and S. Midorikawa, *Phys. Rev.* **D92**, 023004 (2015), 1502.03916.
 - [8] L. Wolfenstein, *Phys. Rev.* **D17**, 2369 (1978).
 - [9] S. T. Petcov, *Phys. Lett.* **B434**, 321 (1998), hep-ph/9805262.
 - [10] E. K. Akhmedov, M. Maltoni, and A. Yu. Smirnov, *JHEP* **05**, 077 (2007), hep-ph/0612285.
 - [11] E. K. Akhmedov, M. Maltoni, and A. Yu. Smirnov, *JHEP* **06**, 072 (2008), 0804.1466.
 - [12] P. Adamson et al. (MINOS), *Phys. Rev. Lett.* **110**, 251801 (2013), 1304.6335.
 - [13] K. Abe et al. (T2K), *Phys. Rev. Lett.* **118**, 151801 (2017), 1701.00432.
 - [14] P. Adamson et al. (NOvA), *Phys. Rev. Lett.* **118**, 151802 (2017), 1701.05891.
 - [15] F. P. An et al. (Daya Bay), *Phys. Rev.* **D95**, 072006 (2017), 1610.04802.
 - [16] R. Wendell (Super-Kamiokande), *AIP Conf. Proc.* **1666**, 100001 (2015), 1412.5234.
 - [17] J. A. Formaggio and G. P. Zeller, *Rev. Mod. Phys.* **84**, 1307 (2012), 1305.7513.
 - [18] A. Friedland, C. Lunardini, and M. Maltoni, *Phys. Rev.* **D70**, 111301 (2004), hep-ph/0408264.
 - [19] A. Friedland and C. Lunardini, *Phys. Rev.* **D72**, 053009 (2005), hep-ph/0506143.
 - [20] T. Ohlsson, H. Zhang, and S. Zhou, *Phys. Rev.* **D88**, 013001 (2013), 1303.6130.
 - [21] A. Esmaili and A. Yu. Smirnov, *JHEP* **06**, 026 (2013), 1304.1042.
 - [22] M. C. Gonzalez-Garcia and M. Maltoni, *JHEP* **09**, 152 (2013), 1307.3092.
 - [23] I. Mocioiu and W. Wright, *Nucl. Phys.* **B893**, 376 (2015), 1410.6193.
 - [24] S. Choubey and T. Ohlsson, *Phys. Lett.* **B739**, 357 (2014), 1410.0410.
 - [25] P. Coloma and T. Schwetz, *Phys. Rev.* **D94**, 055005 (2016), [Erratum: *Phys. Rev.* D95, 079903 (2017)], 1604.05772.
 - [26] J. Liao, D. Marfatia, and K. Whisnant, *Phys. Rev.* **D93**, 093016 (2016), 1601.00927.
 - [27] M. G. Aartsen et al. (IceCube), *Phys. Rev.* **D95**, 112002 (2017), 1702.05160.
 - [28] M. G. Aartsen et al. (IceCube), *Phys. Rev.* **D91**, 072004 (2015), 1410.7227.
 - [29] M. G. Aartsen et al. (IceCube), *JINST* **12**, P03012

- (2017), 1612.05093.
- [30] R. Abbasi et al. (IceCube), Nucl. Instrum. Meth. **A601**, 294 (2009), 0810.4930.
- [31] R. Abbasi et al. (IceCube), Nucl. Instrum. Meth. **A618**, 139 (2010), 1002.2442.
- [32] R. Abbasi et al. (IceCube), Astropart. Phys. **35**, 615 (2012), 1109.6096.
- [33] C. Andreopoulos et al., Nucl. Instrum. Meth. **A614**, 87 (2010), 0905.2517.
- [34] S. Agostinelli et al. (GEANT4), Nucl. Instrum. Meth. **A506**, 250 (2003).
- [35] L. Radel and C. Wiebusch, Astropart. Phys. **38**, 53 (2012), 1206.5530.
- [36] J. H. Koehne, K. Frantzen, M. Schmitz, T. Fuchs, W. Rhode, D. Chirkin, and J. Becker Tjus, Comput. Phys. Commun. **184**, 2070 (2013).
- [37] C. Kopper et al., <https://github.com/claudiok/clsim>.
- [38] M. G. Aartsen et al. (IceCube), Nucl. Instrum. Meth. **A711**, 73 (2013), 1301.5361.
- [39] F. Feroz, M. P. Hobson, and M. Bridges, Mon. Not. Roy. Astron. Soc. **398**, 1601 (2009), 0809.3437.
- [40] A. Hocker et al., PoS **ACAT**, 040 (2007), physics/0703039.
- [41] J. Ahrens et al. (AMANDA), Nucl. Instrum. Meth. **A524**, 169 (2004), astro-ph/0407044.
- [42] F. James and M. Roos, Comput. Phys. Commun. **10**, 343 (1975).
- [43] R. Wendell et al., <http://www.phy.duke.edu/~raw22/public/Prob3++>.
- [44] A. Bodek and U. K. Yang, J. Phys. **G29**, 1899 (2003), hep-ex/0210024.
- [45] T. Katori, P. Lasorak, S. Mandalia, and R. Terri, JPS Conf. Proc. **12**, 010033 (2016), 1602.00083.
- [46] G. D. Barr, T. K. Gaisser, S. Robbins, and T. Stanev, Phys. Rev. **D74**, 094009 (2006), astro-ph/0611266.
- [47] G. J. Feldman and R. D. Cousins, Phys. Rev. **D57**, 3873 (1998), physics/9711021.